Neuron, Vol. 20, 509–526, March, 1998, Copyright ©1998 by Cell Press

Mechanisms of Direction Selectivity in Macaque V1

Margaret S. Livingstone
Department of Neurobiology
Harvard Medical School
Boston, Massachusetts 02115

Summary

Mechanisms underlying direction selectivity were studied in V1 of alert fixating macaque monkeys. Some direction-selective cells showed delayed asymmetric inhibition, some showed a shifting excitatory time course across the receptive field, and some showed both. Both the direction of the spatial offset of the inhibition and the direction of the shift in excitatory response time course correlated with the cells' preferred directionality. The delayed asymmetric inhibition may contribute to the shifting response time course. The data suggest that asymmetric inhibition is the major determinant for directionality in these cells, though both mechanisms could contribute. Based on this physiology, a simple, single-cell model is proposed, consistent with the known anatomy of some direction-selective cells.

Introduction

Some cells in cat and monkey visual cortex show strong preferences for the direction of stimulus motion (Hubel and Wiesel, 1959, 1968). Primary visual cortex is the first stage in the geniculocortical visual pathway where direction selectivity is encountered in these animals, so the mechanisms underlying direction selectivity must be found there. A wealth of studies on direction-selective simple cells in cat striate cortex have concluded that two kinds of mechanisms are most likely to be involved in generating direction selectivity: (1) spatial offsets between excitation and inhibition and (2) shifts across the receptive field in the time course of excitatory responses. Figure 1 diagrams how these two mechanisms could each contribute to direction selectivity. Each mechanism is based on some heterogeneity of response properties across the receptive field, simplified here as two subregions with different responses to flashed stimuli.

Early studies on direction selectivity in anesthetized cat V1 implicated inhibitory mechanisms, because responses to stimuli moving in the null direction were usually smaller than would be predicted from responses to stationary flashed bars (Barlow and Levick, 1965; Goodwin et al., 1975; Ganz, 1984; Ganz and Felder, 1984). Pharmacological studies in cats and primates also have implicated inhibitory mechanisms in direction selectivity (Sillito, 1975, 1977; Sato et al., 1995). How inhibition contributes to direction selectivity is nevertheless still unknown. One simple way that has been proposed for inhibition to contribute to direction selectivity is diagrammed in Figure 1 (left); inhibition is usually imagined to be delayed relative to excitation, so if a stimulus activates the excitatory region first the cell will fire, but if the stimulus crosses the inhibitory region first the excitation is blocked.

Recently, many studies in anesthetized cat have shown that differences across the receptive field in excitatory response timing could contribute to direction selectivity (Movshon et al., 1978; Dean and Tolhurst, 1986; Reid et al., 1987, 1991; McLean and Palmer, 1989; Shapley et al., 1991; DeAngelis et al., 1993; Jagadeesh et al., 1993, 1997; McLean et al., 1994). These studies show that in direction-selective simple cells, the time course of the response to a flashed bar or to a stationary grating changes across the receptive field: responses from the preferred side of the receptive field (the side from which preferred movement begins, subregion "a" in Figure 1) show a slower time course than responses from the null side of the receptive field (the side from which nonpreferred movement originates). When responses from such cells are plotted in space versus time coordinates they show slanted space-time plots. This property is, unfortunately, usually referred to by the confusing term "spatio-temporal inseparability" (Adelson and Bergen, 1985). It is thought that such changes in response time course could contribute to direction selectivity because a stimulus moving in the preferred direction sequentially activates faster and faster responses which will, if the stimulus speed matches the shift in response time course, summate optimally. Stimuli moving in the null direction would first activate fast responses and then slower responses. The peaks of these responses will be asynchronous (Figure 1, right).

Shifting excitatory time course models and spatially offset inhibition models are not mutually exclusive, since inhibition could act synergistically with excitatory mechanisms.

As yet there have been no studies mapping spatio-temporal responses of direction-selective cells in primates. The first experiments in this study were undertaken to see if direction-selective cells in primates, simple or complex, also show oriented space-time maps. To date, all studies on mechanisms of direction selectivity have been in anesthetized animals. This study represents the first receptive-field mapping study of direction selectivity in alert animals. Though it is reasonable to assume no difference in the underlying mechanisms of direction selectivity in anesthetized and alert monkeys, there is an advantage to using alert animals because the higher firing rates often allow one to see inhibition directly (Snodderly and Gur, 1995).

Results

The mapping techniques used in this study combine aspects of the static field map (response-plane) technique (Stevens and Gerstein, 1976; Palmer and Davis, 1981a) and the reverse correlation technique (Jones and Palmer, 1987), with the novel modification that the data are corrected for eye position (Livingstone et al., 1996). Figure 2 shows why the eye-position correction modification was developed. As described by Motter and Poggio (1984), Snodderly and Kurtz (1985), and Snodderly

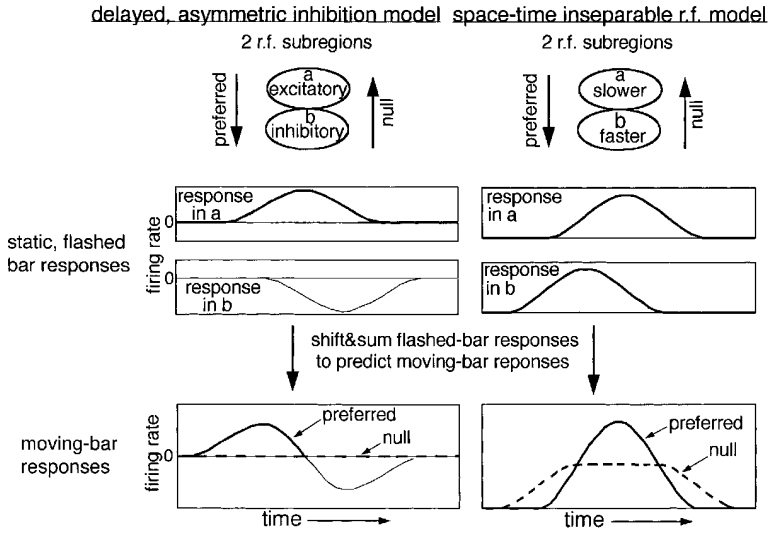

Figure 1. Two Mechanisms that Might Underlie Direction Selectivity

The diagrams show how spatial offsets between excitation and inhibition (left) and differences in excitatory response timing (right) could produce direction selectivity. Both mechanisms are based on differences in response properties across the receptive field, and these differences are stylized here as two subregions, a and b. For both mechanisms the upper two panels show responses to flashed stimuli in two subregions (a and b) of the receptive field; for both models the preferred direction of motion is downward, from subregion a toward subregion b; subregion a represents the preferred side of the receptive field, and subregion b the null side. (Left) A stimulus presented in subregion a gives an excitatory response to a flashed bar, and in subregion b gives a delayed inhibitory response. To mimic a stimulus moving in the preferred direction (a toward b), the response from subregion a is added to a temporally rightward shifted response from subregion b. If a stimulus crosses the excitatory region first, the cell responds and is not inhibited until after the peak of the excitatory response. In the null direction, the inhibitory region is crossed first, so the excitation and inhibition add up in phase, in this example giving no response at all.

(Right) The time course of the response is slower in subregion a and faster in subregion b. To mimic a stimulus moving in the preferred direction (a toward b), the response from subregion a is added to the response from subregion b, with the response from subregion b shifted rightward, because the stimulus arrives there later. Thus, the responses summate in phase. To mimic null-direction stimulation, the response from subregion a is shifted rightward, and the responses add up out of phase. In the simplest linear version of this model, the total spikes in response to either direction of motion are the same, but the peak response is higher in the preferred direction than in the null direction. A threshold operation would then result in different spike totals.

(1987), in both humans and monkeys, even during fixation, gaze position shifts by several tenths of a degree about once every second. Figure 2 shows two typical eye-position records for horizontal (h) and vertical (v) eye position, obtained while the monkey performed a fixation task. The monkey was rewarded for keeping his gaze within 1° of a 0.05° fixation spot. Even while the monkey's gaze was directed at the fixation spot, he made small adjustments in gaze. Because the eye monitor is not completely linear across the visual field, it would be less accurate to try to correct for eye position beyond a few degrees away from the fixation spot. For this study, I therefore used data only from those stimulus presentations when the eyes were within a given distance (1°–3°) of the fixation spot, and within that window corrected the data for eye position. Thus, spikes are correlated with stimulus position on the retina, rather than with stimulus position on the screen.

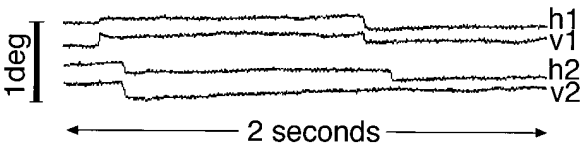

Figure 2. Eye Position Traces from Two Typical 2 s Epochs while the Monkey Fixated on a 0.05° Spot

Each pair of traces shows horizontal (h) and vertical (v) eye position at the indicated spatial and temporal scale. Even though gaze position remains within the 1° gaze limits, the monkey's gaze position varies within that limit. We developed our technique for eye-position-corrected mapping to correct for these small shifts in gaze position. These traces also show that most of the time the monkey's eyes are not moving, so we do not correct for the movements themselves.

For each cell, the optimum orientation was determined using a field of flashing oriented bars, and then subsequent stimuli were always of the optimum orientation. While the monkey held fixation, a small spot or optimally oriented bar having luminance contrast with the background was flashed at random positions covering and immediately surrounding the cell's receptive field. A continuous history was kept of stimulus position, eye position (every 4 ms), and spike occurrence (at 1 ms resolution). Retrospectively, separate average post-stimulus response histograms were calculated for stimulus presentations at each location across the receptive field. A series of such histograms are shown for one direction-selective cell in Figure 3A. This cell's preferred direction of stimulus motion was from locations represented at the bottom of the figure toward locations represented at the top. Going in the preferred direction, this cell showed a progressive shortening of the response onset time across the receptive field and a concomitant increase in response transiency. Also, firing was reduced to below background levels between ~40–60 ms after stimulus onset in the histograms from 3.6°–5.0° across the receptive field. (Note: throughout this paper I will refer to such regions of decreased firing as showing inhibition. It is possible that the decrease in firing does not represent inhibitory input onto the cell being recorded but could be caused by a decrease in excitatory input from an antecedent cell.) Thus, this cell showed properties consistent with both mechanisms diagrammed in Figure 1. In subsequent figures, these same kind of data for other cells will be presented as contour plots in space-time coordinates; a space-time contour plot for these same data is shown overlaid on the histograms in Figure 3B.

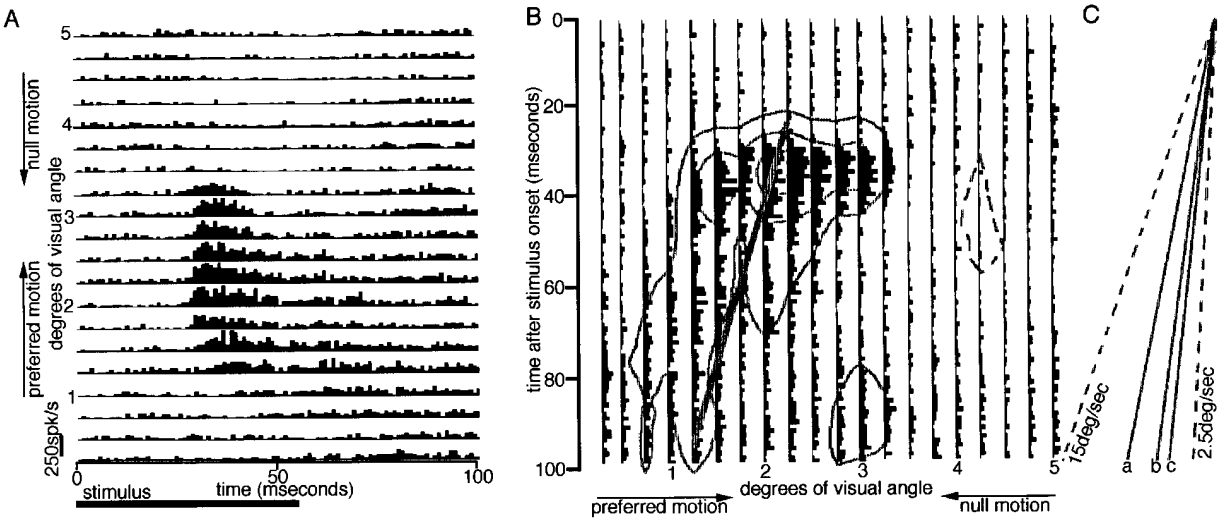

Figure 3. A Series of Responses from a Complex Cell in Alert Macaque V1, Layer 5 or 6, to Flashed Bars, Presented in Random Order at a Series of Positions across the Cell's Receptive Field

This cell was recorded in the roof of the calcarine sulcus in the right hemisphere of an alert macaque monkey. It had an eccentricity of 12° in the lower left part of the visual field.

(A) The entire series of PST histograms represents a 5°-wide segment of the region, with each histogram representing a 0.25°-wide region of receptive field. Each response was assigned to a particular position by calculating the relative bar/eye position at each stimulus onset. Each histogram represents the average response in 1 ms bins of, on average, 75 stimulus presentations. This cell's preferred direction of stimulus motion was from the part of the receptive field represented at the bottom of the figure toward the part of the receptive field represented at the top. Flash duration was 56 ms, and the delay between consecutive flashes was 100 ms.

(B) The same PST histograms are rotated 90° clockwise and overlaid with a space-time contour map for these same data to show how the contour maps in subsequent figures were generated. Solid contour lines indicate increments of two standard deviations above background firing, and dashed contour lines indicate decrements of one standard deviation below background firing. The thick gray line shows the major axis of the moment of inertia. The ratio of the lengths of the major and minor axes was 1.8.

(C) The gray lines show the angle in space-time of various stimulus velocities. "c" represents the speed of a stimulus that would spend 56 ms at each position in (A) and (B). This corresponds to panel 11c in Figure 4. The lines labeled "a" and "b" correspond to stimulus durations used in panels 11a and 11b of Figure 4. The dotted lines represent the indicated speeds, which bracket this cell's range of strongly direction-selective responsiveness.

The space-time plot for this cell shows an overall upward and rightward slope, corresponding to the fact that the response peaks earlier and becomes more transient on going from the preferred to the null side of the receptive field. As diagrammed in Figure 1, a cell whose excitatory response time course shifts across the receptive field can give a larger peak response to one direction of stimulus motion than to the other. The overall response time course at each point, and not just the latency or the time to peak, should be important in predicting how each part of the receptive field will contribute to the response to a moving stimulus. McLean and Palmer (1989) determined the slope of their space-time plots by calculating the spatial centroid at each point in time, and then fit a line to these points. This calculation gives a reasonable approximation of the slope of the function only if the spatio-temporal map is elongated vertically, but if the map is wide or horizontally sloped, the calculated slope will be more vertical than the actual slope of the function. I therefore calculated instead the axis of the moment of inertia (see Appendix). The wide gray line on the contour plot in Figure 3B shows the slope of the major axis of the moment of inertia, which corresponds to the overall slope of the space-time plot. Figure 3C shows how this slope corresponds to the range of velocities over which this cell was direction selective.

This cell showed the same direction preference for dark bars as for light bars. It was a complex cell, in that regions that responded to light bars spatially coincided with regions that responded to dark bars. Hubel and Wiesel (1962) described spatially nonuniform complex cells, but they did not use both black and white stimuli, to distinguish between a nonuniformity of off and on regions versus a nonuniformity of excitation and inhibition. Here, although on and off regions overlap, excitation and inhibition are spatially offset.

Twenty-nine direction-selective cells were similarly mapped with flashed bars (Figure 4). These space-time plots show each cell's response to an optimally oriented bar presented at 20 positions across a 5°-wide region covering the receptive field. The vertical axis is time after stimulus onset, and the horizontal axis represents eye position-corrected stimulus position at stimulus onset. The plots are oriented so that for each cell, the preferred direction of stimulus motion is represented as going from left to right; that is, in each panel, the preferred side of the receptive field is at left and the null side is at right. For each cell, solid contour lines represent increments of two standard deviations above background firing, and dotted contour lines represent decrements of one standard deviation below background firing.

The space-time plots for the cell shown in Figure 3

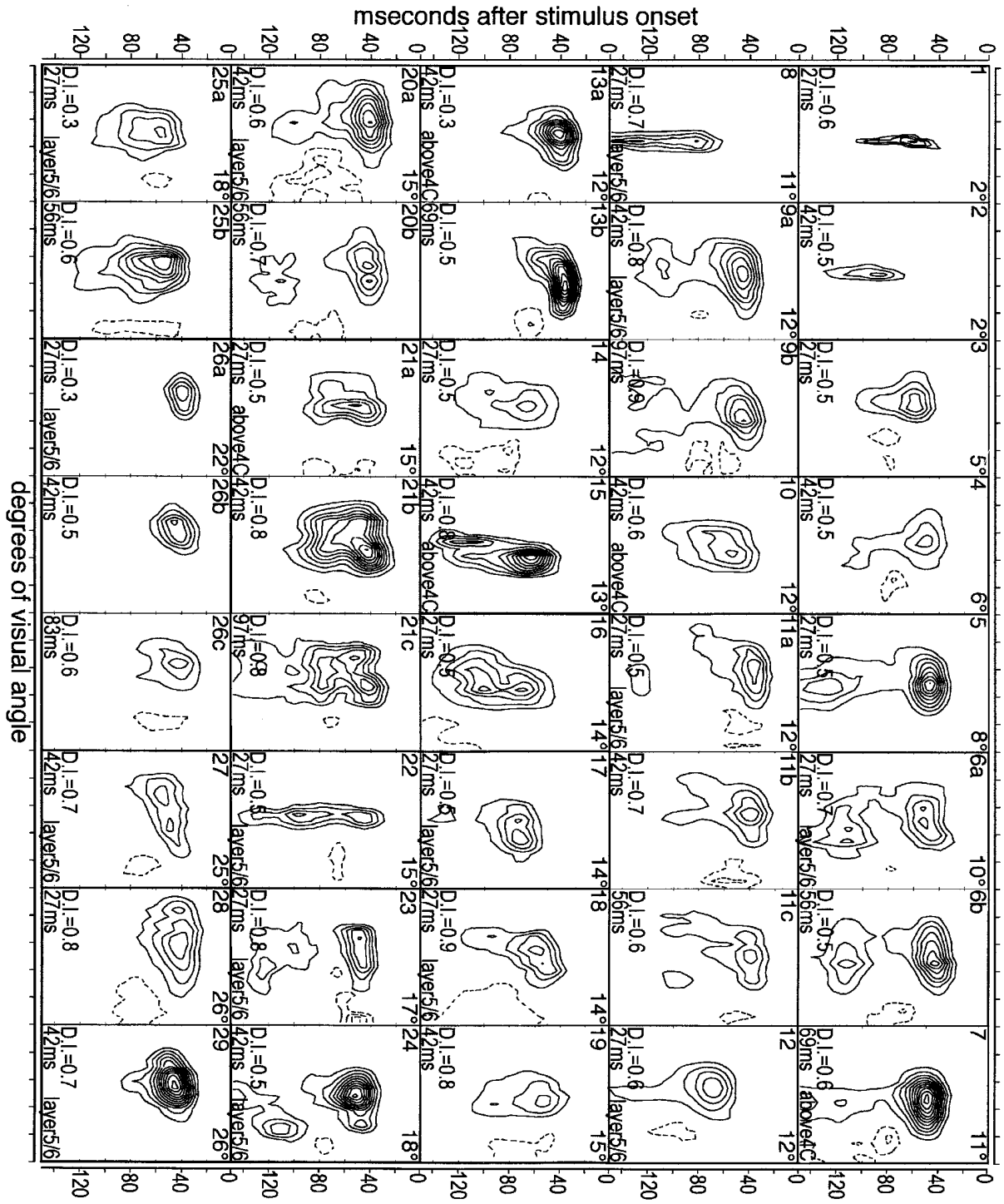

Figure 4. Space-time Plots of Responses from 29 Strongly Direction-Selective Cells in Alert Macaque V1

The horizontal axis represents position across the receptive field (perpendicular to the preferred orientation), with the preferred direction of motion represented as going from left to right. The width of each panel represents 5° of visual angle. PSTHs were calculated for each of 20 stimulus positions, based on the relative bar/eye position at stimulus onset. Each cell was stimulated with an optimally oriented flashed light bar. Each map represents at least 50 (and for most cells more than 100) stimulus presentations at each of the 20 locations and at least 1000 spikes collected. The vertical axis is time after stimulus onset. Solid contour lines represent increments of two standard deviations above background firing, and dashed contour lines represent decrements of one standard deviation below background firing. Each cell is numbered in the upper left corner, so that the same cells can be referred to in subsequent figures. Some cells were studied with more than one stimulus duration, as indicated. Cells are plotted in increasing order of eccentricity, as indicated in the upper right corner of each panel. The lower left corner of each panel lists the cell's direction index (D. I.) and the stimulus duration in ms. (D. I. = preferred response − null response/preferred response + null response; using a smoothly moving bar at a speed that would correspond to spending the same amount of time as the

are in Figure 4, panels 11a–11c. The responses are quite transient, and there are only small differences between responses to different duration stimuli, though all three stimulus durations show the same shortening of response time course in the preferred direction across the receptive field, and all three show evidence of below-baseline firing 40–60 ms after stimulus onset in the null side of the receptive field. For this cell, the gradual shift in response timing is evident as an upward and rightward slope in each space-time plot, and the inhibition on the null side of the receptive field is shown by the dotted contours. By inspection, many other direction-selective cells show slanted space-time plots, and the orientation of the slant is usually up and to the right; that is, the response peaked sooner and was often more transient on going from the preferred toward the null side of the receptive field. This is similar to what was previously found for simple cells in the anesthetized cat (Reid et al., 1987, 1991; McLean and Palmer, 1989; Shapley et al., 1991; DeAngelis et al., 1993; McLean et al., 1994). Many of these direction-selective cells also show an asymmetric region of inhibition on the null side of the receptive field. This inhibitory response usually occurred slightly later than the excitatory response. No cells showed the reverse arrangement of excitation and inhibition with respect to direction preference. Some cells did not show any slant in their space-time plots (3, 4, 19, 24, and 25), though these cells did show a region of inhibition on the null side of the receptive field.

All the cells were tested with both light bars and dark bars, and they all showed the same direction preference for both contrasts (though some cells showed varying degrees of direction selectivity to dark bars). All but one of these cells were complex, in that the dark-bar and light-bar excitatory response regions overlapped, and the light-bar and dark-bar inhibitory regions, if present, also overlapped. Cell 13 was a simple cell, with spatially separate light-bar and dark-bar excitatory regions.

For comparison, space-time plots of 40 nondirectional complex cells are shown in Figure 5. Because these cells showed no direction selectivity, the left-right orientation of the graphs is arbitrary. None of the space-time plots of the nondirectional cells were noticeably slanted, and none showed the asymmetric inhibition seen in many of the direction-selective cells. Some did show delayed inhibition, as shown by the dotted contours, but the inhibition was approximately symmetric across the receptive field.

To quantitate the impression that the space-time plots of many of the direction-selective cells are slanted in a direction corresponding to the preferred direction of motion, whereas the plots of nondirection-selective cells are not, I calculated the axis of the moment of inertia for each plot in Figures 4 and 5 (see appendix). Since the space-time plots of some cells were almost round (such as the first cell in the last row of Figure 5), in those cells the calculated slope is irrelevant. For plots that are elongated, the major axis is longer than the minor axis; for plots that are round, the major and minor axis lengths are equal, so the ratio of the major and minor axes can be used to differentiate the elongated plots from those that are essentially round. Figure 6 shows the slant of these maps plotted in polar coordinates: each point corresponds to one cell, the angle corresponds to the angle of the major axis of the moment of inertia, and the radius corresponds to the ratio of the lengths of the major and minor axes minus 1. In this way, the points corresponding to the unslanted maps cluster at the vertical and horizontal axes, the points for the round maps cluster at the origin, and the points for the slanted maps lie in either the left or right quadrant. By inspection, the points for most of the nondirectional cells lie on the vertical axis or near the origin, while points for many of the directional cells lie in the right quadrant. The fact that there are no direction-selective cells that fall well in the left quadrant is consistent with the observation that most of the direction-selective spatio-temporal maps slant to the right, corresponding with the cells' preferred direction.

McLean and Palmer (1989) and Reid et al. (1991) compared the slants of the space-time plots of cat simple cells with each cell's preferred direction and velocity and found a good overall match. I did not make a thorough study of these cells' velocity tuning, but most cells were tested with smoothly moving bars at 1.25°, 2.5°, 5°, 10°, 15°, and 20°/s. Most of the cells gave direction-selective responses to stimuli moving between 1.25° and 15°/s; only three cells were directional at 20°/s. This range of velocities is bracketed by the gray lines in Figure 6. The spatio-temporal slants of many of the direction-selective cells fall outside this range, suggesting that the shifting response time course may not be the major determinant of direction selectivity in these cells. The space-time plots of some of the cells in the present study (e.g., 11, 13, 18, and 24 in Figure 4) show regions with different slants, as is sometimes seen in the space-time plots of direction-selective simple cells in cat V1 (McLean and Palmer, 1989; DeAngelis et al., 1993; McLean et al., 1994; Emerson, 1997; Reid et al., 1997). The more horizontal component of these plots, and the similarly horizontal slopes of cells such as 23, 27, and 28 correspond to a stimulus velocity of about 200°/s. This is a much higher stimulus velocity than the cells' optimal stimulus velocity, which was on average 10°/s for cells with eccentricities between 10° and 15°. This preferred velocity correlates better with the slope of the tails of the space-time plots of many of the cells or with the more vertical slopes seen in cells 2, 8, 15, 16, or 22. Thus, although the direction of the slant usually correlated well with these cells' direction preference, the slope did not always correlate with the velocity range over which the cells were direction selective.

In order to evaluate the contribution of asymmetric inhibition and slanted space-time characteristics to direction selectivity, I measured how well the flashed-bar

flashed bar duration at each of the 20 positions.) The lower right corner of each panel shows if it was clear if the cell was recorded in layer 5 or 6, or above layer 4C. Layer 5/6 cells were identified by being within 500 μm of the receptive-field jump that indicates going from the opercular cortex to the roof of the calcarine sulcus. Cells indicated as being above layer 4C were probably in layer 4B, and were recorded in the calcarine sulcus, after passing through a region of high spontaneous activity, with monocular responses that lacked orientation selectivity.

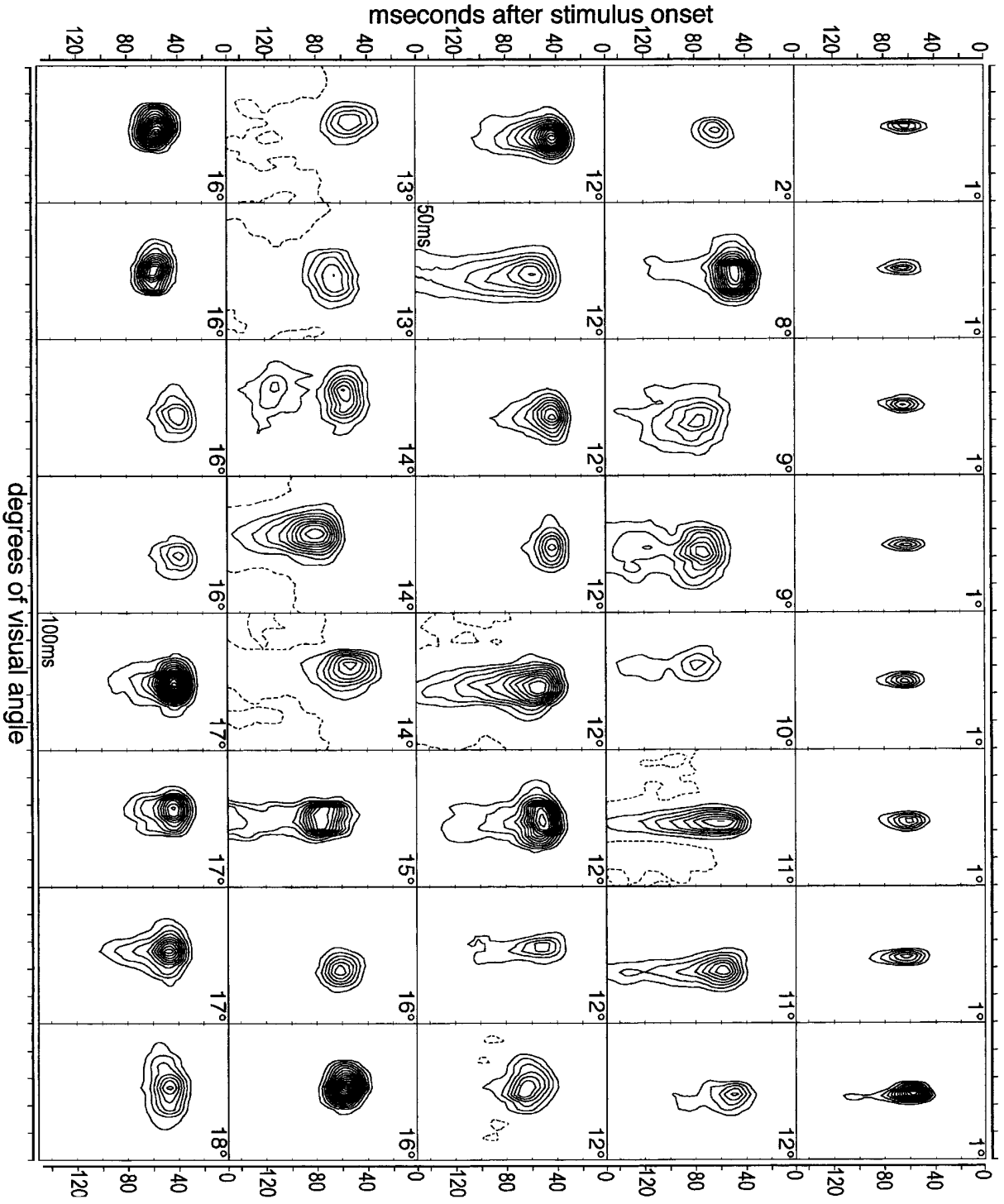

Figure 5. Space-time Plots of Responses from 40 Nondirectional Cells

Each cell was stimulated with an optimally oriented light bar. The horizontal axis represents position across the receptive field (perpendicular to the preferred orientation) Left/right orientation is arbitrary. The width of each panel represents 5° of visual angle. PSTHs were calculated for each of 20 stimulus positions, based on the relative bar/eye position at stimulus onset. The vertical axis is time after stimulus onset. Solid contour lines represent increments of two standard deviations above background firing, and dashed contour lines represent decrements of one standard deviation below background firing. Cells are plotted in increasing order of eccentricity, as indicated in the upper right corner of each panel. Stimulus duration was 27 ms, unless indicated otherwise in the lower left corner of the panel. Each cell was stimulated with an optimally oriented flashed light bar. Each map represents at least 25 (and for most cells more than 100) stimulus presentations at each of the 20 locations and at least 1000 spikes collected.

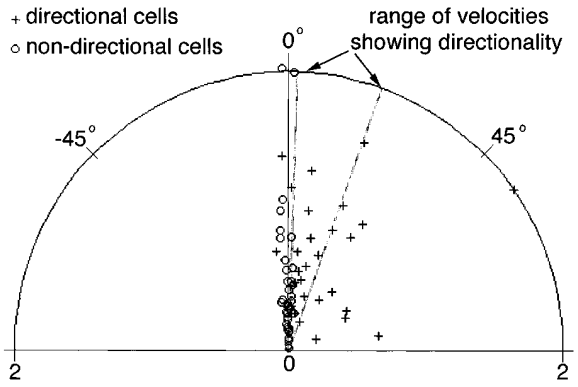

Figure 6. Polar Plot of Orientation of the Major Axis of the Moment of Inertia of the Space-Time Plots of Cells in Figures 4 and 5

Circles indicate nondirectional cells, and crosses represent direction-selective cells. The angle of each point represents the angle the major axis made with the vertical. The radius represents the ratio of the lengths of the major and the minor axis minus 1; maximum ratio = 2. For direction-selective cells for which data for more than one stimulus duration were available, the angles and ratios were averaged. The gray lines bracket the average range of velocities showing strong direction selectivity.

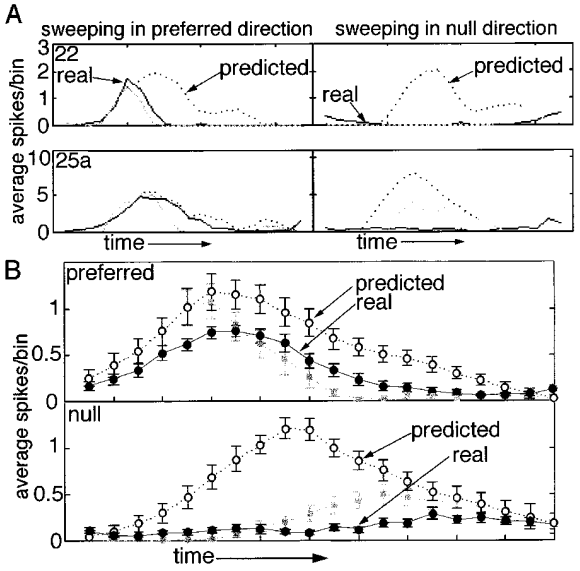

Figure 7. Responses to the Apparent Movement Stimulus Compared to Responses Predicted from Flashed-Bar Stimuli

(A) Real and predicted responses calculated from flashing bar data for two direction-selective cells (numbers in upper left corner refer to cell numbers in Figure 4). Solid lines show averaged responses to the (real) apparent movement stimulus, moving in the preferred direction (left panels) or the null direction (right panels). Apparent movement responses were collected while the monkey fixated, and data were accepted only if the monkey's gaze was within 1° of the fixation spot for the entire stimulus sweep, but the data were not corrected for eye position. Dotted lines show the response predicted for the same stimulus, using responses from identical bars flashed for the same duration, but in random spatial order. PSTHs were calculated for each of 20 stimulus positions, based on the relative bar/eye position at stimulus onset. Averaged responses (including both excitatory and inhibitory components) to randomly flashed bars were shifted in time, to mimic a sequential presentation of stimuli at each location. The shifted responses were then summed to give the predicted response for a bar flashed at each position sequentially. Dashed gray lines show responses predicted from flashed-bar data, with additional inhibition calculated by subtracting the left half of each excitatory response map (mirror reversed) from the right half.

(B) Averaged responses for 15 cells in which a comparison was made between an apparent movement stimulus (real) and responses predicted from flashed-bar stimuli. Solid lines represent responses to the apparent movement stimulus moving in the preferred direction (upper panel) or null direction (lower panel). Dotted lines represent average responses predicted by shifting and summing flashed-bar responses to mimic sequentially presented bars. Dashed gray lines represent average responses predicted from flashed-bar data, with additional inhibition calculated by assuming symmetrical excitation. Error bars represent standard error of the mean.

responses predicted responses to an apparent motion stimulus consisting of the same flashed bars presented in rapid sequence in order across the receptive field. The apparent-movement stimulus consisted of 20 spatially sequential stimulus flashes of the same duration as the randomly presented stimuli, presented to the same 20 receptive-field locations represented in the space-time maps, and produced vivid apparent movement. Responses to the apparent movement stimulus were about the same in the preferred direction as responses to a bar moved as smoothly as possible (given the monitor refresh rate) at the same overall speed, but the responses in the nonpreferred direction were usually smaller for the smoothly moving stimulus. To compare the randomly presented flashing bar responses to the apparent movement responses, 200-ms-long average poststimulus time histograms (PSTHs) to the randomly presented bars at each of the 20 receptive-field locations were shifted temporally to correspond to a given speed of movement in either the preferred or null direction. To calculate a "predicted response," these shifted responses were then simply summed for each time bin (Figure 7A, dotted lines; Reid et al., 1987; McLean and Palmer, 1989).

Figure 7A shows real (solid lines) and predicted (dotted lines) responses for two of the direction-selective cells studied in this way (ignore the gray lines for the moment). For many cells, the moving-bar response predicted from the flashed-bar responses is not smaller for the null direction than for the preferred (it is even sometimes larger). This is probably because, as mentioned above, the slope of the space-time plot often did not match the cell's preferred velocity. An additional 12 cells were examined in this manner (Figure 7B), and all showed the same result: the predicted preferred response was about the same as, or slightly larger than, the real response for movement in the preferred direction, but the predicted null response was much larger than the real response for movement in the null direction. This difference implies that inhibition plays an important role in generating direction selectivity by decreasing the response in the null direction. This idea is further supported by the observation that for some cells, the response to the apparent movement stimulus, moved in the null direction, was smaller than the response to a single flashed bar in the center of the receptive field. The conclusion that inhibition decreases the response in the null direction is in agreement with a large number of previous studies in anesthetized cat (Palmer and

Davis, 1981b; Ganz, 1984; Ganz and Felder, 1984; Emerson et al., 1987; Reid et al., 1987; Shapley et al., 1991; Tolhurst and Dean, 1991). As shown in Figure 1, one very simple way to generate inhibition that is more effective for null-direction stimuli would be to have a receptive field with a region of delayed asymmetric inhibition located on the null side, and this is seen in many of the direction-selective cells in Figure 4.

The fact that the response predicted by summing the shifted flashed-bar responses overestimates the null response for the real moving bar means that the measured decrease in firing below background in response to the flashed bar underestimates the actual inhibition. It would not be surprising if the inhibition were larger than what was measured, since with extracellular recording inhibition can be measured only as a decrement in firing rate, and even a very large inhibitory event can only reduce the firing rate to zero, and not below. As summarized in the discussion, when similar comparisons (between predicted and real responses) were made for cat simple cells it was also necessary to assume an unmeasured inhibitory input. The assumption usually made is that light-bar inhibition exists in the off-region, and that it is temporally identical and of equal but opposite magnitude to the dark-bar excitatory response actually measured there. Because the cells in this study were mostly complex, and did not show spatially separate light- and dark-bar excitatory regions, I could not make the same assumption. Nevertheless, the presence of a measurable region of inhibition on the null side of many space-time plots, and the large notch on the null side of many of the excitatory regions (cells 4, 6, 7, 9, 18, and 20 in Figure 4) suggested that the shape of the excitatory response map might be sculpted by inhibitory processes.

Therefore, in an attempt to explain both the decrease in the null-direction response and the shape of the spatio-temporal maps, I calculated the inhibition needed to produce the observed spatio-temporal map from a spatially symmetric one. To do this, the spatial middle of the excitatory response was calculated by finding the center of the first 5 ms of the excitatory response. Then, the left half of this response map was mirror reversed and subtracted from the right half of the response. This difference represents how much excitation would need to be subtracted from a symmetrical response to obtain the actual response. For most of the direction-selective cells, the observed spatio-temporal map could be accounted for by a combination of a spatially symmetric excitatory response and a delayed, spatially offset inhibitory response. For almost all the cells examined, the inhibition needed to give the observed response map from a symmetrical excitation was on the null side of the receptive field, delayed compared to the excitation, and larger and closer to the excitatory region than the small inhibition (if any) actually measured. When this additional inhibition was included in the calculations comparing moving bar responses to responses predicted from flashing bar responses, the null responses matched much better (dashed gray lines in Figure 7). Therefore, it is possible that a region of inhibition on the null side of the receptive field accounts for both the direction selectivity and the shape of the spatio-temporal map. That is, the upward and rightward slope of the excitatory space-time map could be a result of a symmetrical excitatory input with a delayed inhibitory bite taken out of one side of it.

Predictions from a Model with Asymmetric Inhibition

Barlow et al. (1964) and Barlow and Levick (1965), studying direction-selective units in the rabbit retina, similarly found that responses to stimuli sequentially flashed in the null direction were usually smaller than responses to the same bars flashed individually, implying that inhibition must be involved in generating the null-direction response. They also found that cells were direction-selective throughout the receptive field, implying the existence of direction-selective subunits throughout the receptive field. Barlow and Levick reasoned that if the null-direction inhibition were due to a spatial offset between excitation and inhibition within a subunit, there should be a region on the preferred side of the receptive field where there was no direction selectivity, and they indeed observed this. I do not have the spatial resolution to determine whether there are multiple subunits within a receptive field, but in eight strongly direction-selective cells, I did do a similar experiment to ask if spatially offset inhibition could contribute to direction selectivity. A single light-bar stimulus was moved smoothly back and forth across a 5°-wide region covering the cell's receptive field while the animal held fixation. Then, keeping the sweep of the bar constant, a larger and larger fraction of the null side of the stimulus sweep was occluded. As more and more of a cell's activating region was occluded (always from the null side) the response in the preferred direction got smaller, but the null-direction response got larger. The data from this experiment were not corrected for eye position, but data were collected only if the monkey kept his gaze within 1° of the fixation spot for the entire sweep. Figure 8A shows results typical of all the cells tested, with the the smallest increment in the observed null response pictured in panel iii. Integrated responses to each direction of motion under a series of partial occlusion for all eight cells cells are shown in Figure 8B, and average changes in total response are shown in Figure 8C. For several of the cells tested, when a significant fraction of the null side of the activating region was occluded, the cell became almost completely nondirectional.

The fact that the null-direction response got larger when part of the receptive field was occluded is consistent with the presence of a region of inhibition on that side of the receptive field. The fact that the preferred-direction response did not generally get larger further implies that the inhibition is not activated, or is not activated soon enough, by stimuli moving in the preferred direction. This could happen either if the inhibition were delayed relative to the excitation (as is seen in many of the direction-selective cells in Figure 4), or if the inhibition were itself direction-selective and activated only by stimuli moving in the null direction. If the inhibition is delayed relative to excitation, we would expect some loss of direction selectivity anywhere in the receptive field for stimuli that are briefer either because they traverse a smaller distance or because they move faster.

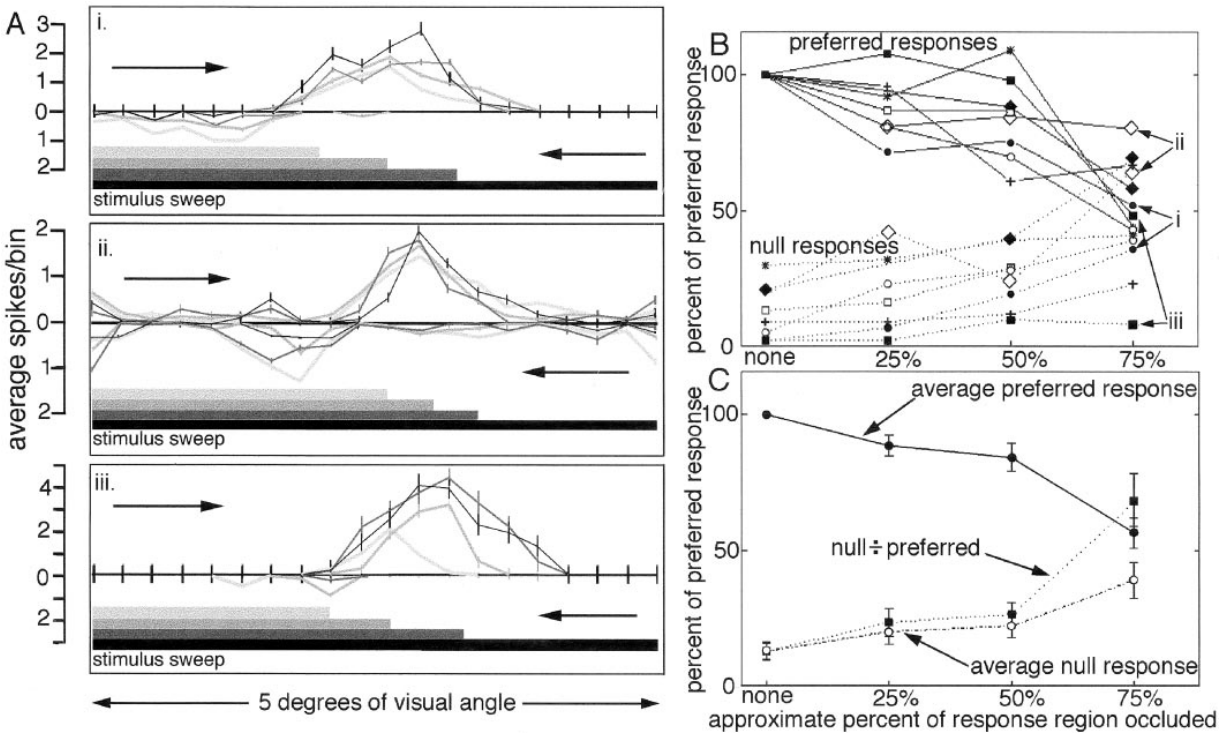

Figure 8. Responses to Partially Occluded Bar Motion

(A) Responses to moving bars in only part of the receptive field for three direction-selective cells. For each cell, average responses to preferred motion are shown on top (with time going from left to right), and average responses to null-direction motion are shown upside-down (with time going from right to left). Data were collected only if the monkey's gaze was within 1° of the fixation spot for the entire stimulus sweep. Data were not corrected for eye position. Bars of different grays below each set of graphs indicate the part of the visual field over which the bar was visible; the rest of the traverse of the bar was occluded. Responses for each bar excursion are coded by gray level.

(B) Individual total responses for all eight cells tested. Responses of the three cells from (A) as indicated. For each cell, the total number of spikes for each direction of stimulus motion, under each condition of stimulus occlusion, were summed. The width of the activating region was measured using the moving bar stimulus. Then fractions of that region, plus the entire bar sweep to the null side of the stimulus sweep, were occluded. Thus, the timing of the stimulus sweep remained identical for all conditions. The estimates of the size of the occluded region must be approximate because the monkey's fixation was not perfect, so the absolute size of the activating region was not known.

(C) Average responses for all eight cells tested for each occlusion condition. The ratio of the null to the preferred response (as a percentage) is also shown.

Indeed, most cells tested with a bar moving at 20°/s showed loss of directionality without complete loss of responsiveness.

Rationale for Final Set of Experiments

Fifteen of the 29 direction-selective cells in this study could be assigned with some certainty to layer 5 or 6, because they were recorded within 300 μm of the shift in receptive-field location on going from superficial (opercular) cortex, where receptive fields are foveal or parafoveal, into the roof of the calcarine sulcus, where receptive fields are more peripheral (Daniel and Whitteridge, 1961). There is also a characteristic preceding short distance of white matter, where no cellular activity is encountered. Furthermore, the extracellular recordings for most of these deep-layer direction-selective cells had very large spikes against a low background, suggesting that the cells themselves were large; many of these cells were held for several hours, also suggesting that they were large (Gur et al., 1997, Soc. Neurosci., abstract).

There is a population of very large, direction-selective, MT-projecting cells at the top of layer 6—the Meynert cells (Meynert, 1872; Lund et al., 1976; Spatz, 1975; Rockland and Pandya, 1979; Tigges et al., 1981; Movshon and Newsome, 1996). LeGros Clark (1942), Lund (1973), Fries (1983, Inves. Ophthal. Vis. Sci., abstract), and Winfield et al. (1983) all describe Meynert cells as having asymmetrical basal dendrites, with a single dendrite often extending hundreds of micrometers in one direction within layer 6. The black cell in Figure 9 is copied from a drawing of a Meynert cell by Cajal (1899) and clearly has asymmetric basal dendrites. Layer 4B cells also often show asymmetrical basal dendritic fields (Elston and Rosa, 1997).

The presence of an asymmetrical dendritic field in a geniculate-input layer suggests a simple model for generating such a cell's direction selectivity that is consistent with the data presented so far. Figure 9 shows a model based on this anatomy. A cell with an asymmetrical dendritic field has excitatory retinotopic inputs located primarily on the dendrites, and relatively denser inhibitory inputs on the cell body. It has been shown that for both cat and monkey V1 pyramidal cells, inhibitory

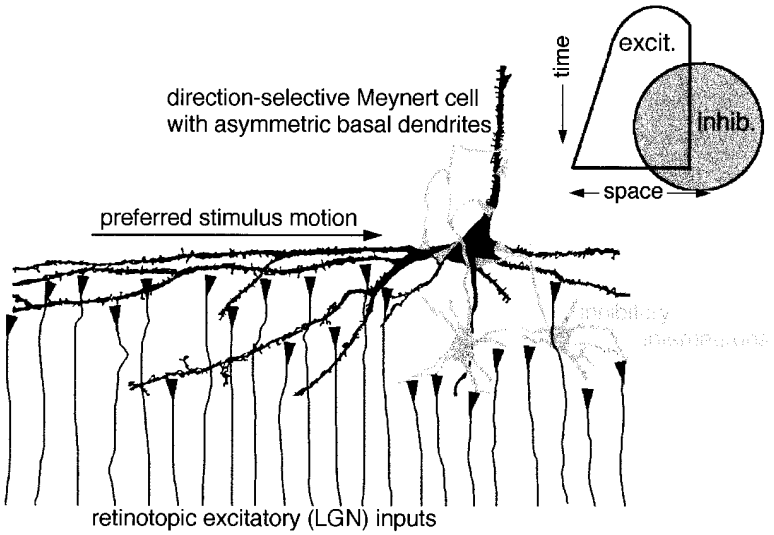

Figure 9. Model of a Cell that Would Be Expected to Show Direction Selectivity

The cell is copied from a drawing by Ramon y Cajal (1899) of a Meynert cell from layer 6 of a human infant. Note the asymmetry of the basal dendrites. Synapses onto this cell are shown schematically as black (excitatory) or gray (inhibitory) triangles. It is postulated that the relative proportion of inhibitory synapses onto the cell body is higher than onto the dendrites. The excitatory inputs are proposed to be retinotopic, not necessarily from the LGN. The model is based only on the cell body and basal dendrites. Influences from the large apical dendrites are not taken into account in this model. The inset shows the kind of spatio-temporal plot that might be expected from such a cell.

inputs are relatively denser on the cell body and proximal dendrites than on distal dendrites, whereas excitatory inputs tend to synapse more onto distal dendrites (Colonnier, 1981; Freund et al., 1983; Beaulieu and Colonnier, 1985, Beaulieu, et al., 1992). For Meynert cells, it is reasonable to suppose the inputs onto different regions of the cell and dendritic field are from the LGN, as shown, but for layer 4B cells, retinotopic inputs could come from layer 4C. This kind of distribution of retinotopic inputs would predict a cell with excitatory and inhibitory inputs from different regions of the visual field. Because of dendritic conduction delays, the model also predicts a shifting response time course across the receptive field, becoming faster going from the preferred toward the null side. That is, responses from the tips of the dendrite would be expected to be slower than responses from inputs nearer the cell body (Rall, 1964).

This model predicts that the major basal dendrite should be oriented parallel to the cell's preferred direction of motion and that it should extend away from the cell body toward the cell's preferred side. This model also predicts a space-time plot that looks something like the diagram at the top of Figure 9. We can make two further simple assumptions: (1) extracellular recording sites are likely to be near the soma, and (2) most cells will have receptive fields that reflect the retinotopy of the inputs to that layer. If these assumptions are true, we can predict that, on average, (1) the cell-body part of the directional cell's receptive field (which should correspond to the short latency transient part of the response) should have the same receptive-field location as other nearby cells, and (2) that the part of the receptive field reflecting inputs onto the long asymmetrical dendrite (which should correspond to the longer latency, sustained part of the excitatory response) should be spatially offset, toward the preferred side of that cell's receptive field. To see if any cells showed such spatial offsets, I compared receptive-field locations of direction-selective cells and surrounding nondirectional cells. Surprisingly, not only some, but most, strongly direction-selective cells tested, in both layer 6 and layer 4B, showed receptive-field offsets consistent with this model. I tested this three different ways.

Tests of Model's Receptive-Field Mapping Predictions

In the first series of experiments, whenever I encountered a well-isolated direction-selective unit, I used a flashing bar stimulus to obtain eye position-corrected reverse correlation maps separately for the direction-selective unit and the lower voltage activity (the background hash) in the same electrode—recorded simultaneously using two different window discrimination levels. I assume that the background hash should reflect the local retinotopy. Reverse correlation maps at a series of times after stimulus onset (delays) were calculated by taking each spike, looking back in time a given delay, and assigning that spike to the relative bar/eye position at that time (Jones and Palmer, 1987). For all 12 strongly direction-selective units tested in this way, the background hash was not direction selective. Figure 10 shows reverse correlation maps at a series of delays for three direction-selective units compared to their background hash. (Note: because elongated bars were used as stimuli, the shape of each map is largely determined by the stimulus shape, not the receptive-field shape, but the location of the center of the map should reflect the receptive-field location, at that delay. These are space-space maps, not space-time plots, as shown in previous figures.) For each direction-selective cell shown, the response map changes position as the delay is varied. In each case, the direction the peak moves is related to the cell's direction selectivity: the peak of the response map migrates toward the cell's preferred side with longer delays. In Figure 10, the maps for the background hash recorded from the same electrode as the direction-selective cells are located at about the same location as the peak of the direction-selective map at short delays, but at longer delays, the direction-selective map shifts (toward its preferred side), while the nondirectional hash map does not shift. Of the 12 direction-selective cells tested in this way, 10 showed clear shifts in their reverse correlation maps, and two did not. Of the 10 cells that showed shifts, all showed the same relationship between the cell and the background hash, consistent with the predictions of the proposed model. (Had these 10 cells been plotted as in Figure 4 of the

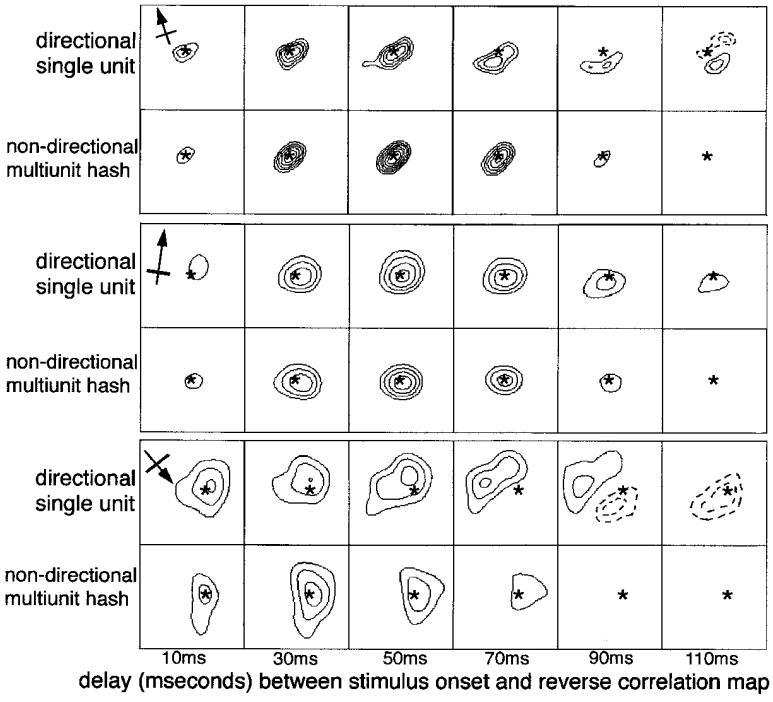

Figure 10. Reverse-Correlation Maps for Three Direction-Selective Cells Compared to Background Hash Recorded in the Same Electrode at a Series of Delays

The direction-selective single unit and the background hash were differentially recorded using window discriminators. Each panel represents 3° × 3° degrees of visual angle, oriented in visual space as the monkey would see it (that is, up in the map represents up in the monkey's visual field). The asterisk position within each set of panels represents the same point in visual space and is simply there for spatial reference. For each spike in the spike train, the computer looks back in time the indicated delay and assigns that spike to the most recent bar/eye position at that time. Each map therefore represents the response density for a given bar/eye position (in 20% increments above background) at a given time interval before each spike. The cells and hash were simultaneously mapped using a light bar, shown to scale for each pair, that flashed at random positions in and around the cells' receptive fields. The bar was the optimum orientation for the direction-selective cell, and is shown to scale in the first panel of each series, with the preferred direction as indicated. The stimulus duration in these experiments was 27 ms, with 27 ms between each stimulus presentation, so the responses at 10 ms do not represent ridiculously short latencies but rather the fact that the stimulus position changed only every 56 s, and the eyes do not change position very frequently. The responses at 10 ms represent the earliest responses to stimulus onset at each position, and the later delay times represent longer latency responses. The first two recordings were at 4° eccentricity, and the last recording was at 12° eccentricity.

previous part of the study, they would have shown upwardly slanted space-time plots; the two cells that did not show shifts would have shown nonslanted plots.) A shift in the response map could of course be predicted from the sloped space-time plots of other direction-selective cells. Any direction selectivity model that invokes a shifting time course across the receptive field would similarly predict that the reverse correlation map should shift toward the preferred side at longer delays, but the model I have proposed in addition predicts that there should be a consistent relationship between the response map of the direction-selective cell and the maps of nearby cells.

A second way to ask this same question is to map pairs of cells with pairs of closely spaced electrodes. In a series of experiments recording with pairs and triplets of electrodes, in which the tips of the electrodes were less than 0.3 mm apart, single direction-selective units and one to three nondirectional single units or multiunits were recorded and stimulated simultaneously to obtain reverse correlation maps. Figure 11 shows 15 such sets of reverse correlation maps. The reverse correlation maps were calculated at a 60 ms delay, to maximize the predicted spatial offset. At shorter delays the offset was usually less, as would be predicted from the model. Some of the maps overlapped, but most showed some spatial offset between the direction-selective cell and the nearby nondirectional cell(s). When there was a spatial offset, it was usually such that the map of the direction-selective cell was offset toward its own preferred side. Because there is scatter in receptive-field location even within a cortical column (Hubel and Wiesel, 1974), we would expect the receptive fields of simultaneously recorded nearby cells to be spatially offset to some extent, but the direction of the offset should be random if it is only due to receptive-field scatter. The pattern observed here is not random, and is, in fact, the pattern predicted by the model I have proposed.

Lastly, I made 1–2 mm-long penetrations, mapping activity every 50–100 μm, roughly perpendicular to the surface of the cortex, to look at the pattern of receptive-field position within columns. The peak positions of the reverse correlation maps, calculated at 60 ms delays, are shown in Figures 12A–12C for three such penetrations. Each experiment consisted of recording from two electrodes with tips of the same length, less than 300 μm apart, advanced together through the cortex. Each recording series was begun when the receptive-field location jumped from parafoveal to around 10° out in the visual field, indicating that the electrode had entered the roof of the calcarine sulcus. Each series therefore probably begins with cells in layer 6 (shown at the bottom of each panel) and progresses upward toward more superficial layers. The horizontal axis represents receptive-field location in the dimension perpendicular to the average preferred orientation of all the cells in the penetration. Scatter in the other dimension is not shown. The lines show a least squares fit with the receptive fields of the nondirectional cells for each electrode penetration. Strongly direction-selective activity is indicated by arrowheads, pointing in the preferred direction. Because I sampled activity every 50–100 μm, it is probable that some of the apparent clustering of direction selectivity may simply represent recording of the same unit

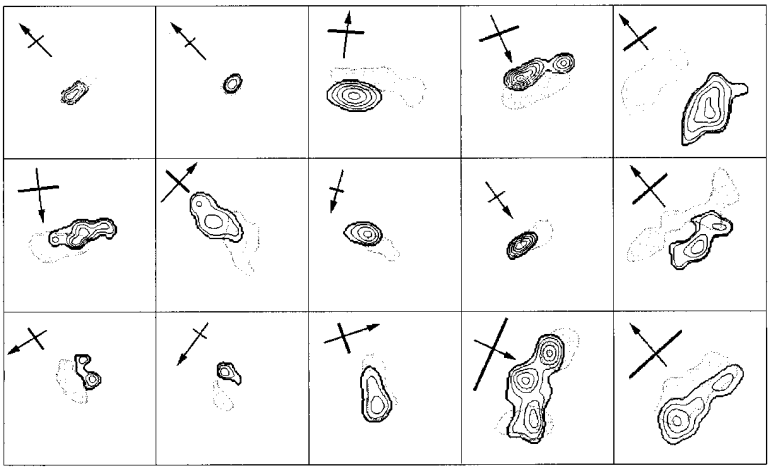

Figure 11. Reverse-Correlation Maps for Direction-Selective Cells Compared with Nearby Nondirectional Cells Recorded with a Second Electrode Less than 300 μm away

For each pair, one cell was a well-isolated single unit that was strongly directional. The other unit was either a single unit or multiunit hash and did not show direction selectivity. All cells were recorded in the roof of the calcarine sulcus and had receptive-field eccentricities between 10° and 15°. Each panel represents 5° × 5° of visual field, oriented as in visual space. The direction-selective cell in each pair is shown in black, and the nondirectional cell(s) in gray. The cells were mapped using a light bar, shown to scale for each cell pair, that flashed at random positions in and around the cells' receptive fields. The cells usually had similar orientation preferences, and the bar used was the optimum orientation for the direction-selective cell. The preferred direction for each of the direction-selective cells is indicated in each panel. Stimulus duration was 27 ms, with 27 ms between stimuli. The reverse correlation maps represent firing density at each relative bar/eye position 60 ms before each spike. The maps are elongated because the stimuli were elongated, and therefore do not represent receptive-field shape but do accurately represent receptive-field location.

at more than one recording site. By inspection, in any given penetration, the long latency responses of the direction-selective cells tended to be offset toward their own preferred side, as predicted by my model. Figure 12D shows a histogram of long latency response map peak distance from the regression line for nondirectional cells (closed bars) and for direction-selective cells (open bars). On average, the peaks of the direction-selective cell response maps were offset by 0.3° toward their preferred side.

One can, with some certainty, identify layers in alert monkey striate cortex on physiological criteria. In these penetrations, layer 6, where direction-selective cells are frequently found, can be identified by the jump in receptive-field location. One can tentatively identify layer 4C by high spontaneous firing, lack of orientation selectivity, and monocularity (Poggio et al., 1977; Livingstone and Hubel, 1984; Maunsell and Gibson, 1992; Peterhans and von der Heydt, 1993; Snodderly and Gur, 1995). Several of the penetrations probably passed through layer 4C and into layer 4B, where direction-selective cells were again encountered. As shown in Figures 12B and 12C, spatial offset of receptive fields toward the preferred side was observed not only in layer 6, but also in layer 4B.

Discussion

Previous Studies on Directionality in the Primate

There have been no previous spatio-temporal mapping studies on direction-selective cells in primate V1, either anesthetized or alert. Hamilton et al. (1989) measured responses of simple cells in anesthetized cat and anesthetized monkeys to drifting sine wave gratings. They calculated from the moving grating responses what spatio-temporal maps would look like if they assumed the cells fit a linear quadrature model, but spatio-temporal properties were not determined directly. Gaska et al. (1994) used white noise stimuli to determine second order space-time spectra (essentially two-bar interaction strengths) for complex cells in anesthetized macaque V1. They found that the two-bar interaction kernels correctly predicted many aspects of cells' responses to drifting sine wave gratings, including direction selectivity. Since they did not show single-bar response maps, the data presented here in no way disagree with their results, though one might assume from their concentration on second-order interactions that nothing of interest was observed in the single-bar (first order) kernels.

Previous Evidence for Asymmetric Inhibition

Several lines of evidence from studies in anesthetized cat indicate that asymmetric inhibitory mechanisms may be used to generate direction selectivity. Palmer and Davis (1981b; their Figure 10) and Emerson et al. (1985) show examples of cells in which a region of light-bar inhibition is seen on the null side of the receptive field. Using conditioning stimuli in the nondominant eye, Innocenti and Fiore (1974) and Hammond and Kim (1994) mapped excitatory and inhibitory regions in direction-selective cells in anesthetized cat and found spatially offset excitatory and inhibitory regions, with the inhibitory region lying toward the null side of the receptive field. Ganz and Felder (1984), Ganz (1984), Emerson and Gerstein (1977), and Emerson et al. (1987) presented pairs of bars in sequence in either the preferred or the null direction and found that the response to a single bar was smaller when it was preceded by a stimulus from the null side than it would be to the second bar in isolation. Pharmacological studies also indicate that inhibitory mechanisms are probably involved in generating direction selectivity (Sillito, 1975, 1977; Sato et al., 1995).

Previous Spatio-Temporal Studies on Direction-Selective Complex Cells

Most previous physiological studies on direction selectivity were done on simple cells in anesthetized cat. Emerson and colleagues (Emerson et al., 1987, 1992)

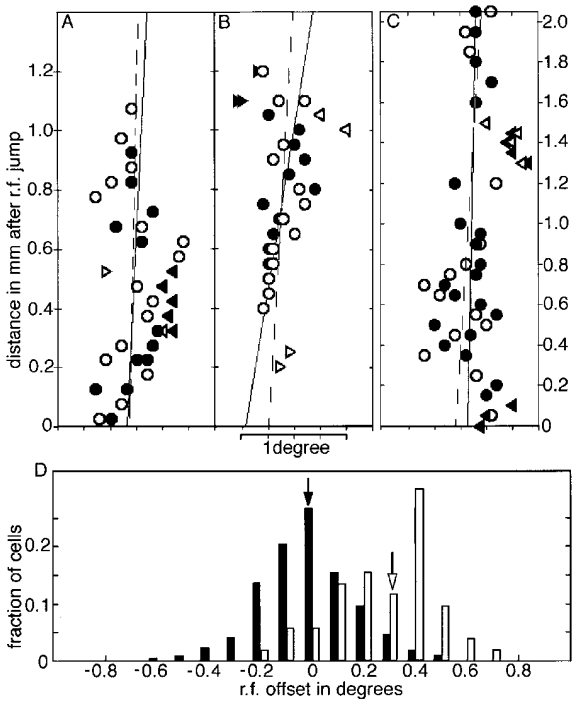

Figure 12. Receptive-Field Location of Direction-Selective Cells and Nondirectional Cells in Penetrations Perpendicular to the Surface of the Cortex

The cells were mapped as in the previous two Figures. Stimulus duration was 27 ms, with 27 msonds between stimuli. The reverse correlation maps were calculated using a delay of 60 ms.

(A–C) Three typical two-electrode penetrations through the roof of the calcarine sulcus. The location in the visual field of the peak of each recorded response map at a delay of 60 ms was determined. The vertical axis is distance in mm the electrode traveled after the jump in receptive-field location, indicating that the electrode had passed into layer 6 of the roof of the calcarine sulcus. Note the different scales for (C) versus (A) and (B). The average orientation of all the cells in each electrode penetration was determined. (There were often differences in the preferred orientation between the two electrodes and often a drift in preferred orientation with depth.) Then the position along an axis perpendicular to that average orientation was measured for each peak locus, which is represented by the position on the x-axis in each plot. That is, receptive-field scatter in the dimension perpendicular to the average optimum orientation is shown, and scatter in the orthogonal dimension is not shown. The width of each panel represents 1.5° of visual angle in the dimension perpendicular to the average preferred orientation. Open and closed symbols indicate activity recorded by the two electrodes. Circles indicate the receptive-field location of the peak of each nondirectional locus and arrowheads represent directional loci, with the direction of the arrowhead indicating the cell's preferred direction. On physiological criteria, the pair of penetrations shown in (A) probably did not pass completely through layer 4C; layer 4C activity was probably recorded between depths of 0.4 and 0.9 mm in (B); layer 4C activity was probably recorded between 0.5 and 1.1 mm in (C). Each line shows the least squares fit for the nondirectional cells in one penetration (dotted lines correspond to penetrations represented by open symbols, and solid lines correspond to closed symbols).

(D) Histogram of spatial offset of direction-selective cells (open bars, n = 54) and nondirectional cells (closed bars, n = 222) for nine pairs of penetrations similar to, and including, those shown in (A) through (C). For each recording locus, the distance to the nondirectional regression line was measured. For direction-selective cells, this distance was considered positive if the offset was toward the preferred side of the cell's receptive field (consistent with the model) and negative if the opposite. For nondirectional cells, one direction of spatial offset for each pair of penetrations was arbitrarily designated as positive. The closed bars show the scatter of receptive-field locations for nondirectional cells. The median offset is, by definition, zero (closed arrow) because the regression lines were calculated from the same data. The open bars show the fraction of direction-selective cells at each spatial offset. The median spatial offset for the direction-selective cells was 0.3° (open arrow), indicating that the direction-selective cells tended to have receptive fields that were spatially offset from surrounding nondirectional cells and that the spatial offset was usually toward each cell's preferred side.

analyzed a small number of complex cells in anesthetized cat V1 and reported that single-bar response maps did not show either slanted space-time properties or response heterogeneity across the receptive field that might explain their direction selectivity. They could see direction-selective mechanisms only when they looked at 2-bar interactions. However, the complex cell shown in Figures 1 and 4 of Emerson et al. (1992) actually does show a space-time slant, though the slope would correspond to a much faster velocity than the cell's optimum velocity (as was seen for some cells in this study).

Previously Proposed Mechanisms for Generating Oriented Space-Time Properties

For a cell to have slanted space-time properties it must have timing differences between different parts of the receptive field. Such timing differences could arise intracortically or from inputs with different temporal properties.

Quadrature Model

The most popular theory for how slanted space-time characteristics might arise is that the cell sums inputs from antecedent cells having spatially and temporally offset receptive fields (Adelson and Bergen, 1985; Watson and Ahumada, 1985). The two-component slopes of some of the space-time plots shown here, and seen in several other studies (McLean and Palmer, 1989; Reid et al., 1991, 1997; DeAngelis et al., 1993; McLean et al., 1994; Emerson, 1997), are similar to the simple-cell space-time filter calculated by Adelson and Bergen (1985) using only two separable input filters (their Figure 10). Nevertheless, the data presented here are not consistent with the quadrature model because (1) this model does not predict a region of inhibition on the null side of the receptive field, and (2) this model predicts slanted space-time plots for simple cells, but predicts uniform space-time plots for complex cells (Emerson et al., 1992).

Inputs with Different Temporal Properties

Saul and Humphrey (1990) proposed that slanted space-time profiles could arise from geniculate inputs with different temporal properties, i.e., lagged and nonlagged cells (Mastronarde, 1987; Humphrey and Weller, 1988). The timing differences reported for geniculate cells in primates are probably too short to explain the slopes observed here (Irvin et al., 1986; Spear et al., 1994; Wang et al., 1997, Soc. Neurosci., abstract).

Dendritic Conduction Delay

Rall (1964) showed that, based on simple cable properties, the voltage change seen at a neuron's cell body

from a distal dendritic synaptic input would be slower and smaller than the voltage change from an equivalent synaptic input at a more proximal dendritic location. Therefore a single class of inputs, with homogeneous temporal properties, could produce responses with different time courses depending on how far from the soma the inputs synapse. Rall also showed that the somatic potential change as a result of a series of dendritic inputs activated at certain time intervals should be larger when the activation order is toward rather than away from the cell body. This would produce direction selectivity only if the dendritic field were asymmetric, as proposed here. At this eccentricity (12°) the cortical magnification factor in V1 is about 0.4 mm/° (Van Essen et al., 1984). An active dendritic conduction velocity of 0.3 m/s (see Johnston et al., 1996) would predict a delay of only a few ms across the receptive field of the cell shown in Figure 3. Therefore, active dendritic conduction could explain the most horizontal spatio-temporal slopes of Figure 4 but would be a bit too fast to explain the longer delay tails. However, dendritic signal propagation is complex and a number of factors, including thresholding, might contribute to conduction delays (Rall, 1964; Johnston et al., 1996). A modification of the model, suggested by David Ferster, which might better explain the quite long latencies seen in the tails of the space-time plots, would be if the inputs to the cell body and proximal dendrites were direct, but inputs to more distal dendrites were cortically delayed. The receptive-field offset predictions of this modified model would be essentially the same.

Inhibitory Mechanisms in Linear Models

As has been reported in many previous studies in the cat, I also found that the sum of temporally shifted flashed-bar responses was larger than the total response to the same bars flashed in sequence in the null direction. For sine wave gratings, this implies either an underestimation of inhibitory mechanisms or the presence of a thresholding operation (Jagadeesh et al., 1993, 1997). For the comparisons of flashed-bar responses made here, where the comparison stimuli are precisely equivalent except for the order of presentation, an overestimation of the magnitude of the null response can only imply that the inhibition (or the withdrawal of excitation) was larger than was measured. I suggested that one way to estimate an invisible inhibition would be to assume that the underlying excitatory receptive field is spatially symmetric, and I calculated the spatially offset inhibition needed to produce the observed receptive field from a symmetrical one. By including this estimated inhibitory input, predicted responses in both null and preferred directions matched measured responses to real moving stimuli much better. If the model is correct, however, and the dendritic fields of many direction-selective cells are asymmetric, then the assumption that the underlying excitatory input field is symmetric would not be valid. Since there is no way of estimating the excitatory-input asymmetry at this point, this way of estimating the actual inhibition has to remain a rough guess.

Most previous studies comparing predicted with real responses also include an unmeasured inhibitory component. In some studies using flashing bars, inhibitory responses were not measured directly, but were assumed to be equal in magnitude but opposite in sign to responses to flashed bars of the opposite contrast (McLean and Palmer, 1989; McLean et al., 1994). The equivalent assumption is also made in studies comparing static and moving sine wave gratings when half-wave rectification is assumed (Reid et al., 1987, 1991; Tolhurst and Dean, 1991). Indeed, linear analysis does not distinguish between excitation by one phase of a binary stimulus and inhibition by the other (see Reid et al., 1997). Though simple-cell receptive fields are organized in a mutually antagonistic, push-pull fashion (Hubel and Wiesel, 1962; Palmer and Davis, 1981a; Glezer et al., 1982; Ferster, 1988), the excitation and opposite-contrast inhibition within a subregion are actually not usually balanced (Heggelund, 1986).

The intracellular study of Jagadeesh et al. (1993, 1997) showed that membrane-voltage responses to moving gratings in both preferred and null directions can be predicted accurately from responses to stationary temporally modulated gratings. This indicates that excitatory and inhibitory changes in membrane voltage do sum linearly, but the spike generating mechanisms are not linear. This does not mean that inhibitory mechanisms are not involved in generating direction selectivity, it means only that inhibitory voltage changes add linearly with excitatory voltage changes, and that no significant amount of shunting inhibition is involved.

The Question of Subunits

Many previous studies on direction-selective cells showed that direction selectivity is present throughout the receptive field, even in quite small subdivisions of the receptive field, implying that there must be multiple direction-selective subunits (Barlow and Levick, 1965; Bishop et al., 1973; Emerson and Gerstein, 1977; Ganz, 1984; Ganz and Felder, 1984; Emerson et al., 1987). Barlow and Levick (1965) proposed that direction selectivity in the rabbit retina was generated by a series of direction-selective subunits combining excitation and inhibition, with the inhibitory region delayed relative to excitation and spatially offset toward the null side of the receptive field. The occlusion experiment suggests that the number of subunits in the cells studied here is small, conceivably as small as one. If a cell had a large number of identical subunits, one would expect the size of the maximum occlusion-induced null response to be only a fraction of the maximum preferred response (Barlow and Levick, 1965), but some of the cells tested here showed occlusion-induced null responses that were half as large, or larger, than the nonoccluded preferred response. Because there are multiple overlapping subunits in their model, there is no overall spatial segregation between excitation and inhibition, as seen here, though the main difference might only be in the number of subunits.

Conclusions

There is no reason for the results obtained here on complex cells in alert monkeys to be the same as previous results from simple cells in anesthetized cats, unless mechanisms underlying direction selectivity are general.

Yet despite the differences between cat and monkey, simple and complex cells, and anesthetized and alert preparations, the two major characteristics of direction-selective cells observed in cat (shifting excitatory response time course and asymmetric inhibition) have been found, in this study, to characterize direction-selective cells in the macaque. Because some direction-selective cells showed a shifting time course, others showed asymmetric inhibition, and still others showed both, one could conclude that either mechanism could underlie direction selectivity in the primate.

I have proposed a single-cell model for direction selectivity in which both mechanisms could contribute to directionality. The essential features are an asymmetric dendritic field and a differential localization of excitatory and inhibitory inputs onto the dendrites and cell body. The asymmetric dendritic field and localization of inhibitory inputs to the cell body would result in a spatial offset between excitation and inhibition. I propose that the shifting response time course on the preferred side of the receptive field is due to delays accumulated from dendritic conduction and thresholding, while the abrupt transiency on the null side is due to delayed inhibition. Indeed, the increased transiency of the excitatory response on the null side of the receptive field is consistent with a delayed inhibitory mechanism, even in those cells that do not show below-baseline firing in that part of the map. This is more parsimonious than supposing that the slanted space-time properties arise from inputs with multiple different time courses varying in both latency and transiency.

A direction selectivity mechanism due entirely to "spatio-temporal inseparability" would tend to be direction-selective over a narrow range of velocities, roughly corresponding to the spatio-temporal slope. In contrast, a direction selectivity mechanism arising from asymmetric inhibition is likely to show a broader range of directional velocities. The direction selectivity mechanism proposed here is based on both properties, and therefore should be even more robust.

Others have sought and failed, even with better techniques, to find correlates between dendritic morphology and receptive-field properties, such as orientation selectivity, in cat V1 (Martin and Whitteridge, 1984). Nevertheless, no one has reported looking for correlations between direction selectivity and dendritic morphology, so my proposed hypothesis does not contradict any published studies. Obviously, the critical experiment to test this hypothesis would be to correlate directly the basal dendritic morphology and orientation in visual space with a cell's known direction selectivity. We plan to do this.

The proposed model is obvious, given the reported asymmetry in dendritic morphology in Meynert cells and the known differential distribution of excitatory and inhibitory synapses on pyramidal cells. Meynert cells are not, however, an abundant cell type, so the question remains whether this model might apply to other direction-selective cells. That the model fits the spatio-temporal maps and receptive-field spatial offsets of most of the directional cells mapped (including cells recorded superficial to layer 4C), and not of just a small minority, suggests that this model might apply to other kinds of directional cells besides Meynert cells. Consistent with this, Elston and Rosa (1997) recently reported that layer 4B cells also often show asymmetric basal dendritic fields. The 4B basal dendritic fields were not asymmetric in their tangential extent, as were those of Meynert cells, but they did show an asymmetry in dendritic branch density, with 40% of 4B cells showing dendritic branching at least twice as dense in one direction as in any other direction.

Experimental Procedures

Single units were recorded extracellularly with fine electropolished tungsten electrodes coated with vinyl lacquer (Hubel, 1957). Usually, recordings were made simulanteously from two electrodes placed 100–500 μm apart. Extracellularly recorded signals were amplified, band-pass filtered (1–10 kHz), and fed into a dual window discriminator (BAK Electronics). Unless stated otherwise, recordings were from single units, as determined by monitoring the size and shape of the unit and from the refractory period seen in the interspike interval histogram. Spike times were recorded with 1 ms resolution.

Data were collected from three male rhesus macaque monkeys. Eye position was monitored with a search coil in a magnetic field as previously described (Judge et al., 1980) with an eye monitor manufactured by DNI. At the beginning and end of each recording session, the eye monitor was calibrated by rewarding the monkey for following a fixation spot that appeared randomly at each of the four corners and at the center of a $10^\circ \times 8^\circ$ rectangle on the monitor. Eye positions were collected at 10 Hz while the monkey followed the fixation spot to map the calibration. The eye monitor was adjusted until the recorded eye position corresponded as precisely as possible to the spot positions. Afterward, if necessary, a simple distortion algorithm was used to align precisely the eye position at all five fixation spots; all positions in between were distorted linearly. With the three monkeys so far, the distortion across 10° of visual angle was minimal. During recording of neuronal activity, eye position was sampled at 250 Hz.

For each cell, the optimum orientation was determined using a field of flashing oriented bars. Poststimulus response histograms, space-time maps, and reverse correlation (space-space) maps were obtained by using an optimally oriented bar flashed at random positions in and around the cell's activating region (Jones and Palmer, 1987). Stimulus duration was between 27 and 97 s; interstimulus interval was between 27 and 200 ms. A continuous record of spike time (at 1 ms resolution), stimulus position, and eye position (at 4 ms resolution) was recorded. Afterwards, the data could be read back as relative stimulus/eye position (which corresponds to stimulus position on the retina) at any time before any given spike (Livingstone et al., 1996).

To obtain poststimulus time histograms (PSTHs), 300 ms epochs following stimulus onset at each given relative bar/eye position (which corresponds to stimulus position on the retina) were averaged together. Thus, PSTHs were generated for each stimulus position on the retina at stimulus onset. For the PSTHs, we only correct for eye position at stimulus onset because (1) responses are transient so stimulus onset position is probably most critical, (2) the eyes move only about once per second and there are many stimulus presentations per second, and (3) it is not clear how one should go about correcting for eye movements within a stimulus presentation. To calculate space-time plots and reverse correlation space-space plots, background firing rate was subtracted for each point. Background firing rate was determined as the average firing rate for the first 20 ms after stimulus onset for all stimulus positions. I did not use an unstimulated firing rate for background because the firing rate is somewhat elevated during the random stimulus presentation, particularly with short interstimulus intervals. Reverse correlation (space-space) maps (Jones and Palmer, 1987; De Angelis et al., 1993) were calculated by taking each spike, looking back in time a given delay, and assigning that spike to the relative bar/eye position at that time. For the space-time maps, data were binned into twenty 0.25°-wide spatial bins, and in the temporal dimension were averaged and smoothed, using a Gaussian filter (15 ms). For the space-space plots, data were collected at a 0.05° resolution, and were smoothed with a two-dimensional Gaussian of 0.3°.

For some cells, light- and dark-bar stimuli (27 and 0.002 cd/m^2, repectively) were mapped in intermixed trials on an intermediate gray background (7 cd/m^2); for other cells, the light and dark stimuli were presented in separate trials, on reversed contrast backgrounds (white bar and white background = 10 cd/m^2; black bar and background = 0.002 cd/m^2). Though it is obviously best to present light and dark stimuli intermixed on an intermediate luminance background, there were reasons for not always doing this. In early experiments the first priority was to obtain the spatio-temporal map for light-bar stimuli, and it was never clear whether the cell would be held long enough to get dark-bar responses as well. Also many cells, particularly direction-selective ones, often responded to the refresh rate of the monitor when there was a large gray background, making those maps very noisy.

Simple cells were defined as cells that showed spatial segregation of light-bar and dark-bar excitatory regions; complex cells were defined as cells in which light-bar and dark-bar excitatory regions overlapped (Hubel and Wiesel, 1962).

During mapping, the monkey was rewarded with a single drop of juice or water for keeping his gaze for 2–4 s within 1° of a small (0.05°) spot on the monitor. The monkey maintained fixation intermittently for several hours. For the spatio-temporal maps shown in Figures 4 and 5, data were used only if the monkey's eye position was within 2° of the fixation spot at the time of stimulus onset; within that window, data were corrected for eye position.

For moving bar stimuli, an optimally oriented bar was moved smoothly, or flashed in a series of positions, across the cell's receptive field while the monkey fixated a 0.05° spot. Responses were collected only when the monkey's gaze was within 1° of the fixation spot for the entire stimulus sweep but were not corrected for eye position. Cells were defined as direction-selective cells only if the response to one direction of stimulus motion was at least three times larger than the response to the other direction.

A Zeos 120 mHz Pentium computer was used for stimulus generation and data collection. Stimuli were presented on a 21 in NEC multisynch monitor with a 72 Hz refresh rate, and the monitor screen was 65 cm in front of the monkey.

All experimental and surgical procedures conformed to NIH and USDA guidelines and were approved by the Harvard Medical Area Standing Committee on the Use of Animals.

Appendix

Calculation of the Slope of Space-Time Plots

(From Landau and Lifshitz, 1976, with help from Doris Tsao.)

This calculation is the standard way of calculating the axes of the moment of inertia of a plane figure.

The calculation is analogous to the line-weighting calculation of McLean and Palmer, 1989, except that it weights the slope equally with respect to both space and time dimensions, and it gives the ratio of elongation of the major and minor axes.

First the background is subtracted, and positive values of the space-time plot are interpolated to give a 100 × 100 x, t matrix representing 5° × 100 ms. The center of mass of the matrix is calculated and assigned position 0, 0 at the center of a 100 × 100 matrix. Then a 2 × 2 matrix A is constructed:

$$\begin{array}{|c|c|} \hline \dfrac{\Sigma z_{x,t} \cdot x^2}{\Sigma z_{x,t}} & \dfrac{\Sigma -z_{x,t} \cdot x \cdot t}{\Sigma z_{x,t}} \\ \hline \dfrac{\Sigma -z_{x,t} \cdot x \cdot t}{\Sigma z_{x,t}} & \dfrac{\Sigma z_{x,t} \cdot t^2}{\Sigma z_{x,t}} \\ \hline \end{array}$$

where $z_{x,t}$ is the value in spikes/s at each point in the matrix, x is the spatial coordinate, and t is the time coordinate. The eigenvectors of this matrix give the basis (coordinate system) in which this matrix would be a diagonal matrix (that is the positions 1, 2 and 2, 1 are zero). This is equivalent to asking about which axis, that goes through the center of mass, is the original matrix balanced. We use MATLAB to calculate the diagonal eigenvalue matrix D and the full matrix V of corresponding eigenvectors of matrix A so that $A \cdot V = V \cdot D$.

Then if (V_1, V_2) is the eigenvector corresponding to the larger eigenvalue, then V_2/V_1 is the slope of the major axis. The slope of the minor axis is perpendicular to that. The ratio of the lengths of the major and minor axes is the square root of the ratio of the two eigenvalues.

Acknowledgments

This work was supported by National Institutes of Health grant RO1 EY10203. David Freeman did all the computer programming; Gail Robertson provided excellent technical support; Clay Reid provided many helpful discussions; and Bevil Conway, Terrence Sejnowski, Raj Rao, John Assad, Lawrence Sincich, Stephen Macknik, Richard Born, David Ferster, Gregory Petsko, and Richard Masland's lab provided insightful criticism of the manuscript; Doris Tsao helped with math.

Received December 8, 1997; revised February 17, 1998.

References

Adelson, E.H., and Bergen, J.R. (1985). Spatiotemporal energy models for the perception of motion. J. Opt. Soc. Am. A. *2*, 284–299.

Barlow, H.B., and Levick, W.R. (1965). The mechanism of directionally selective units in rabbit's retina. J. Physiol. *178*, 477–504.

Barlow, H.B., Hill, R.M., and Levick, W.R. (1964). Retinal ganglion cells responding selectively to direction and speed of image motion in the rabbit. J. Physiol. *173*, 377–407.

Beaulieu, C., and Colonnier, M. (1985). A laminar analysis of the number of round-asymmetrical and flat-symmetrical synapses on spines, dendritic trunks, and cell bodies in area 17 of the cat. J. Comp. Neurol. *231*,180–189.

Beaulieu, C., Kisvarday, Z., Somogyi, P., Cynader, M., and Cowey, A. (1992). Quantitative distribution of GAGA-immunopositive and -immunonegative neurons and synapses in the monkey striate cortex. (area 17). Cerebral Cortex *2*, 295–309.

Bishop, P.O., Goodwin, A.W., and Henry, G.H. (1973). Direction selective sub-regions in striate simple cell receptive fields. J. Physiol. *238*, 25–27.

Cajal, S.R. (1899). Estudios sobre la corteza cerebral humana. Rev. Trim. Micrografica *4*,1–63.

Colonnier, M. (1981). The electron microscopic analysis of the neuronal organization of the cerebral cortex. In The Organization of the Cerebral Cortex. F.O. Schmitt, F.G. Worden and S.D. Dennis, eds. (Cambridge, Massachusetts: MIT Press), pp. 125–151.

Daniel, P.M., and Whitteridge, D. (1961). The representation of the visual field on the cerebral cortex in monkeys. J. Physiol. *159*, 203–221.

Dean, A.F., and Tolhurst, D.J. (1986). Factors influencing the temporal phase of response to bar and grating stimuli for simple cells in the cat striate cortex. Exp. Brain Res. *62*, 143–151.

DeAngelis, G.C., Ohzawa, I., and Freeman, R.D. (1993). Spatiotemporal organization of simple-cell receptive fields in the cat's striate cortex. I. General characteristics and postnatal development. J. Neurophysiol. *69*, 1091–117.

Elston, G.N., and Rosa, J.G.P. (1997). The occipitoparietal pathway of the macaque monkey: comparison of the pyramidal cell morphology in layer III of functionaly related cortical visual areas. Cerebral Cortex *7*, 432–452.

Emerson, R.C. (1997). Quadrature subunits in directionally selective simple cells spatio-temporal interactions. Visual Neurosci. *14*, 357–371.

Emerson, R.C., and Gerstein, G.L. (1977). Simple striate neurons in the cat. II. Mechanisms underlying directional asymmetry and directional selectivity. J. Neurophysiol. *40*, 136–155.

Emerson, R.C., Citron, M.C., Felleman, D.J., and Kaas, J.H. (1985). A proposed mechanism and site for cortical directional selectivity. In Models of Visual Cortex. D. Rose and V. G. Dobson, eds. (New York: John Wiley and Sons), pp. 420–430.

Emerson, R.C., Citron, M.C., Vaughn, W.J., and Klein, S.A. (1987). Nonlinear directionally selective subunits in complex cells of cat striate cortex. J. Neurophysiol. *58*, 33–65.

Emerson, R.C., Bergen, J.R., and Adelson, E.H. (1992). Directionally selective complex cells and the computation of motion energy in cat visual cortex. Vision Res. *32*, 203–218.

Ferster, D. (1988). Spatially opponent excitation and inhibition in simple cells of the cat visual cortex. J. Neurosci. *8*, 1172–1180.

Freund, T.F., Martin, K.A.C., Smith, A.D., and Somogyi, P. (1983). Glutamic acid decarboxylase-immunoreactive terminals of Golgi-impregnated axoaxonic cells and of presumed basket cells in synaptic contact with pyramidal neurons of the cat's visual cortex. J. Comp. Neurol. *221*, 263–278.

Ganz, L. (1984). Visual cortical mechanisms responsible for direction selectivity. Vision Res. 243–11.

Ganz, L., and Felder, R. (1984). Mechanism of directional selectivity in simple neurons of the cat's visual cortex analyzed with stationary flash sequences. J. Neurophysiol. *51*, 294–324

Gaska, J.P., Jacobson, L.D., Chen, H.-W., and Pollen, D.A. (1994). Space-time spectra of complex cell filters in the macaque monkey A comparison of results obtained with pseudowhite noise and grating stimuli. Visual Neurosci. *11*, 805–821.

Glezer, V.D., Tsherbach, T.A., Gauselman, V.E., and Bondarko, V.M. (1982). Spatio-temporal organization of receptive fields of the cat striate cortex. Biol. Cyber. *43*, 35–49.

Goodwin, A.W., Henry, G.H., and Bishop, P.O. (1975). Direction selectivity of simple striate cells: properties and mechanism. J. Neurophysiol. *38*, 1500–1523.

Hamilton, D.B., Albrecht, D.G., and Geisler, W.S. (1989). Visual cortical receptive fields in monkey and cat spatial and temporal phase transfer function. Vision Res. *29*, 1285–1308.

Hammond, P., and Kim, J.-N. (1994). Spatial correlation of suppressive and excitatory receptive fields with direction selectivity of complex cells in cat striate cortex. Proc. R. Soc. Lond. (B) *257*, 179–184.

Heggelund, P. (1986). Quantitative studies of enhancement and suppression zones in the receptive field of simple cells in cat striate cortex. J. Physiol. *373*, 293–310.

Hubel, D.H. (1957). Tungsten microelectrode for recording from single units. Science *125*, 549–550.

Hubel, D.H., and Wiesel, T.N. (1959). Receptive fields of single neurones in the cat's striate cortex. J. Physiol. *148*, 574–591.

Hubel, D.H., and Wiesel, T.N. (1962). Receptive fields, binocular interaction and functional architecture in the cat's visual cortex. J. Physiol. *160*, 106–54.

Hubel, D.H., and Wiesel, T.N. (1968). Receptive fields and functional architecture of monkey striate cortex. J. Physiol. *95*, 215–243.

Hubel, D.H., and Wiesel, T.N. (1974). Uniformity of monkey striate cortex a parallel relationship between field size, scatter, and magnification factor. J. Comp. Neurol. *158*, 295–306.

Humphrey, A.L., and Weller, R.E. (1988). Functionally distinct groups of X-cells in the lateral geniculate nucleus of the cat. J. Comp. Neurol. *268*, 429–447.

Innocenti, G.M., and Fiore, L. (1974). Post-synaptic inhibitory components of the responses to moving stimuli in area 17. Brain Res. *80*, 122–126.

Irvin, G.E., Norton, T.T., Sesma, M.A., and Casagrande, V.A. (1986). W-like response properties of interlaminar zone cells in the lateral geniculate nucleus of a primate (*Galago crassicaudatus*). Brain Res. *362*, 254–270.

Jagadeesh, B., Wheat, H.S., and Ferster, D. (1993). Linearity of summation of synaptic potentials underlying direction selectivity in simple cells of the cat visual cortex. Science *262*, 1901–1904.

Jagadeesh, B., Wheat, H.S., Kontsevich, L.L, Tyler, C.W., and Ferster, D. (1997). Direction selectivity of synaptic potentials in simple cells of the cat visual cortex. J. Neurophysiol. *78*, 2772–2789.

Johnston, D., Magee, J.C., Colbert, C.M., Christie, B.R. (1996). Active properties of neuronal dendrites. Annu. Rev. Neurosci. *19*, 165–186.

Jones, J.P., and, Palmer L. A. (1987). The two-dimensional spatial structure of simple receptive fields in cat striate cortex. J. Neurophysiol. *58*, 1187–1121.

Judge, S.J., Richmond, B.J., and Chu, F.C. (1980). Implantation of magnetic search coils for measurement of eye position: an improved method. Vision Res. *20*, 535–538.

Landau, L.D., and Lifshitz, E.M. (1976). Mechanics, Third Edition. (New York: Pergammon Press), p. 99.

LeGros Clark, W.E. (1942). The cells of Meynert in the visual cortex of the monkey. J. Anat. *76*, 369–376.

Livingstone, M.S., and D. H. Hubel (1984). Anatomy and physiology of a color system in the primate visual cortex. J. Neurosci. *4*, 309–356.

Livingstone, M.S., Freeman, D.C., and Hubel, D.H. (1996). Visual responses in V1 of freely viewing monkeys. Cold Spring Harbor Symp. Quant. Biol. *61*, 27–37.

Lund, J.S. (1973). Organization of neurons in the visual cortex, area 17, of the monkey (*Macaca mulatta*). J. Comp. Neurol. *147*, 455–496

Lund, J.S., Lund, R.D., Hendrickson, A.E., Bunt, A.H., and Fuchs, A.F. (1976). The origin of efferent pathways from the primary visual cortex, area 17, of the macaque monkey as shown by retrograde transport of horseradish peroxidase. J. Comparative Neurol. *164*, 287–303.

Martin, K.A.C., and Whitteridge, D. (1984). The relationship of receptive field properties to the dendritic shape of neurones in the cat striate cortex. J. Physiol. *356*, 291–302.

Mastronarde, D.N. (1987). Two classes of single-input X-cells in cat lateral geniculate nucleus. I. Receptive-field properties and classification of cells. J. Neurophysiol. *57*, 357–380.

Maunsell, J.H., and Gibson, J.R. (1992). Visual response latencies in striate cortex of the macaque monkey. J Neurophysiol. *68*, 1332–1344.

McLean, J., and Palmer, L.A. (1989). Contribution of linear spatio-temporal receptive field structure to velocity selectivity of simple cells in area 17 of cat. Vision Res. *29*, 675–679.

McLean, J., Raab, S., and Palmer, L.A. (1994). Contribution of linear mechanisms to the specification of local motion by simple cells in area 17 and 18 of the cat. Visual Neurosci. *11*, 271–294.

Meynert, T. (1872). Vom Gehirne der Saugethiere. In Handbuch der Lehre von den Geweben des Menschen und der Thiere. S. Stricker, ed. (Leipzig: Whilhelm Engelman), pp. 694–808.

Motter, B.C., and Poggio, G.F. (1984). Binocular fixation in the rhesus monkey spatial and temporal characteristics. Exp. Brain Res. *54*, 304–14.

Movshon, J.A., and Newsome, W.T. (1996). Visual response properties of striate cortical neurons projecting to area MT in macaque monkeys. J. Neurosci. *16*, 7733–7741.

Movshon, J.A., Thompson, I.D., and Tolhurst, D.J. (1978). Spatial summation in the receptive fields of simple cells in the cat's striate cortex. J. Physiol. *283*, 53–77.

Palmer, L.A., and Davis, T.L. (1981a). Receptive-field structure in cat striate cortex. J. Neurophysiol. *46*, 260–76.

Palmer, L.A., and Davis, T.L. (1981b). Comparison of responses to moving and stationary stimuli in cat striate cortex. J. Neurophysiol. *46*, 277–295.

Peterhans, E., and von der Heydt, R. (1993). Functional organization of area V2 in the alert macaque. Eur. J. Neurosci. *5*, 509–24.

Poggio, G.F., Doty, R.W., Jr., and Talbot, W.H. (1977). Foveal striate cortex of behaving monkey single-neuron responses to square-wave gratings during fixation of gaze. J. Neurophysiol. *40*, 1369–1391.

Rall, W. (1964). Theoretical significance of dendritic trees for neuronal input-output relations. In Neural Theory and Modeling. R.F. Reiss, ed. (Palo Alto: Stanford University Press), pp. 122–146.

Reid, R.C., Soodak, R.E., and Shapley, R.M. (1987). Linear mechanisms of directional selectivity in simple cells of cat striate cortex. Proc. Nat. Acad. Sci. USA *84*, 8740–8744.

Reid, R.C., Soodak, R.E., and Shapley, R.M. (1991). Directional selectivity and spatio-temporal structure of receptive fields of simple cells in cat striate cortex. J. Neurophysiol. *66*, 505–529.

Reid, R.C., Victor, J.D., and Shapley, R.M. (1997). The use of m-sequences in the analysis of visual neurons: linear receptive field properties. Visual Neurosci. *14*, 1015–1027.

Rockland, K.S., and Pandya, D.N. (1979). Laminar origins and terminations of cortical connections of the occipital lobe in the rhesus monkey. Brain Res. *179*, 3–20.

Sato, H., Katsuyama, N., Tamura, H., Hata, Y., and Tsumoto, T. (1995). Mechanisms underlying direction selectivity of neurons in the primary visual cortex of the macaque. J. Neurophysiol. *74*, 1382–1394.

Saul, A.B., and Humphrey, A.L. (1990). Spatial and temporal response properties of lagged and nonlagged cells in cat lateral geniculate nucleus. J. Neurophysiol. *64*, 206–224.

Shapley, R., Reid, C.R., and Soodak, R. (1991). Spatiotemporal receptive fields and direction selectivity. In Computational Models of Visual Processing. M.S. Landy and J.A. Movshon, eds. (Cambridge, Massachusetts: MIT Press), pp. 109–118.

Sillito, A.M. (1975). The contribution of inhibitory mechanisms to the receptive field properties of neurones in the striate cortex of the cat. J. Physiol. *250*, 305–329.

Sillito, A.M. (1977). Inhibitory processes underlying the directional specificity of simple, complex and hypercomplex cells in the cat's visual cortex. J. Physiol. *271*, 699–720.

Snodderly, D.M. (1987). Effects of light and dark environments on macaque and human fixational eye movements. Vision Res. *27*, 401–415.

Snodderly, D.M., and Kurtz, D. (1985). Eye position during fixation tasks comparison of macaque and human. Vision Res. *25*, 83–98.

Snodderly, D.M., and Gur, M. (1995). Organization of striate cortex of alert, trained monkeys (*Macaca fascicularis*) ongoing activity, stimulus selectivity, and widths of receptive field activating regions. J. Neurophysiol. *74*, 2100–2125.

Spatz, W.B. (1975). An efferent connection of the solitary cells of Meynert. A study with horseradish peroxidase in the marmoset. Callithrix. Brain Res. *92*, 450–455.

Spear, P.D., Moore, R.J., Kim, C.B.Y., Xue, J.-T., and Tumosa, N. (1994). Effects of aging on the primate visual system spatial and temporal processing by lateral geniculate neurons in young adult and old rhesus monkeys. J. Neurophysiol. *72*, 402–420.

Stevens, J.K., and Gerstein, G.L. (1976). Spatiotemporal organization of cat lateral geniculate receptive fields. J. Neurophysiol. *39*, 213–238.

Tigges, J., Tigges, M., Anschel, S., Cross, N.A., Ledbetter, W.D., and McBride, R.L. (1981). Areal and laminar distribution of neurons interconnecting the central visual cortical areas 17, 18, 19, and MT in squirrel monkey (Saimiri). J. Comp. Neurol. *202*, 539–60.

Tolhurst, D.J., and Dean, A.F. (1991). Evaluation of a linear model of directional selectivity in simple cells of the cat's striate cortex. Visual Neurosci. *6*, 421–428.

Van Essen, D.C., Newsome, W.T., and Maunsell, J.H.R. (1984). The visual field representation in striate cortex of the macaque monkey asymmetries, anisotropies, and individual variability. Vision Res. *24*, 429–48.

Watson, A.B., and Ahumada, A.J. (1985). Model of human visual-motion sensing. J. Opt. Soc. Am. A. *2*, 322–342.

Winfield, D.A., Neal, J.W., and Powell, T.P.S. (1983). The basal dendrites of Meynert cells in the striate cortex of the monkey. Proc. R. Soc. Lond. (B) *217*, 129–139.